JOURNAL OF MATERIALS SCIENCE 28 (1993) 4347–4354

Precipitation of chromium containing phases in aluminide coated nickel-base superalloy single crystals

W. F. GALE*, J. E. KING
Department of Materials Science and Metallurgy, University of Cambridge, Pembroke Street, Cambridge, CB2 3QZ, UK

The precipitation of chromium-containing phases, in both the B2 type β-phase coating matrix (nominally NiAl) and the substrate of high-activity-pack-aluminized single crystals of a nickel-base superalloy, is considered in this paper. An 'edge-on' transmission electron microscopy (TEM) technique is employed to examine the precipitation of $M_{23}X_6$, σ, α-Cr and other phases after coating and diffusion treatment and subsequent post-coating treatment at 850 and 950 °C. Initial precipitation is dominated by the formation of $M_{23}X_6$ in both the coating and substrate, however, in the case of single-crystal substrates the formation of this carbon-rich phase is not sustained. $M_{23}X_6$ precipitation is superceded by the formation of coherent precipitates of the α-Cr phase which effectively retains the basis but removes the superlattice of the β-matrix. Extensive precipitation of α-Cr has the effect of changing the balance of chromium to molybdenum in solution in the β-phase and further precipitation is dominated by σ-phase intermetallics and other Cr–Mo-containing phases.

1. Introduction

Aluminide diffusion coatings are used extensively for the protection of nickel-base superalloys against high-temperature oxidation. However, relatively few detailed studies have been made of microstructural development in these systems. Although initial-coated microstructures have been characterized, most notably by Shen *et al.* for aluminized René 80 [1, 2], a systematic examination of changes in the microstructure of aluminized single crystals with post-coating treatments has not been found. In this regard, even though polycrystalline coatings are produced with both single-crystal and polycrystalline substrates, important differences might be expected in coating microstructures due, for example, to the lower levels of carbon present in single-crystal alloys.

In the present investigation, an examination is made of the precipitation of chromium-containing phases in a high-activity-pack aluminized single-crystal nickel-base superalloy. Chromium is a major alloying addition to the substrate, and considerable quantities of chromium are incorporated in the coating during its formation. Chromium has a relatively low solubility in the β-phase (for example 4 at % for stoichiometric NiAl at 850 °C [3]) when compared to the chromium content of the coating (which is in the approximate range of 5–25 at % Cr [4]). Hence, the precipitation of chromium-containing phases would be expected to be of considerable importance. Indeed, apart from decomposition of the B2 matrix of the coating (which has been addressed by the authors elsewhere [4]), the precipitation of chromium-containing phases is found to be the most important factor in coating-microstructural development.

2. Experimental techniques

Single crystals of a nickel-base superalloy (with principal alloying additions of Co, Cr, Al, Ti, Mo and V) were solution treated for 4 h at 1260 °C, followed by gas fan quenching to 800 °C, and air cooling to room temperature. These specimens were subsequently pack aluminized for 4 h at 870 °C and then subjected to a 1 h diffusion treatment at 1100 °C. A further 16 h ageing treatment (Throughout this paper, the term "aged" is used to refer to the 16 h ageing treatment at 870 °C applied after aluminization and diffusion treatment. Any subsequent treatments are identified as "exposure". "Post-coating treatment" is used to collectively describe ageing and exposure) at a temperature of 870 °C was employed to produce a bimodal distribution of γ′ (nominally Ni_3 (Al, Ti)) in the substrate. An argon atmosphere was employed throughout these treatments.

In addition to examination of specimens in the as-diffusion treated and as-aged conditions, further heat treatments at a temperature of 850 °C were examined. These treatments involved holding times of up to 138 h in either laboratory air or a 10^{-2} Pa vacuum. Samples with standard (nominally 40 μm) thickness coatings were examined. Additional work was conducted on samples with thin (nominally 10 μm) coatings, exposed at either 850 or 950 °C in air for up to 138 h.

* *Present Address*: Materials Engineering Program, Auburn University, Auburn, AL 36849, AL, USA.

0022–2461

Edge-on specimens were prepared from these samples and characterized by the use of transmission electron microscopy (TEM), together with energy-dispersive X-ray analysis (EDS). Coating cross-sectional samples were also examined using light and scanning electron microscopy (SEM) and SEM-based EDS. Further details of the experimental techniques employed may be found elsewhere [4].

3. Results and discussion

Following the microstructural investigations, a number of different layers were observed in the microstructure. These are shown in Figs 1 and 2a; where, in addition to the main coating and the bulk substrate, there are intermediate transitional layers in the coating and substrate adjacent to the coating–substrate interface. At the outer surface of the coating an additional layer is produced where the microstructure of the coating is influenced by the presence of an outer oxide layer. Although the microstructures and sizes of the layers vary as a function of initial coating thickness and subsequent treatment, the layer designations given above may still be applied. Precipitation of a variety of chromium-containing phases was observed after coating and diffusion treatment and also following further post-coating ageing. The formation of major phases is now discussed, as far as possible, in chronological order of their appearance (minor phases that are mostly of importance as nucleation sites for major phases are described together with the relevant major phase).

3.1. $M_{23}X_6$ precipitation

Within the timescale examined (i.e. up to 138 h exposure at 850 °C), $M_{23}X_6$ (for which M is predominantly chromium with some molybdenum, and X is assumed to be carbon) was found to be the predominant chromium-containing phase in standard thickness coated samples. Indeed, in thin coatings, only $M_{23}X_6$ was observed. Generally, attention will be focused on precipitation within the coating; however, in order to understand some of the features of this precipitation, an examination of $M_{23}X_6$ formation in the substrate is required.

3.1.1. Precipitation within the substrate

In the bulk substrate which is unaffected by the presence of the coating, occasional cuboidal $M_{23}X_6$ precipitates (aligned along $\langle 110 \rangle_\gamma$ directions and typically around 200 nm long) were observed; these were cube–cube oriented with the γ-Ni matrix and with the γ′-precipitates (Fig. 2b). Immediately adjacent to the coating, however, a region of chromium enrichment was encountered (presumably as a result of chromium rejection by the growing β-phase during coating formation), in which excess precipitation of $M_{23}X_6$ was produced. In the case of standard thickness coatings (Fig. 2a), these precipitates were essentially elongated versions of the $M_{23}X_6$ in the bulk substrate (with typical lengths of around 500 nm). $M_{23}X_6$ precipitation in the substrate-transition layer was observed both in the coated and diffusion-treated material and in samples subjected to post-coating treatment. However, following 16 h post-ageing exposure at 850 °C, the formation of $M_{23}X_6$ was superceded by that of a σ-phase.

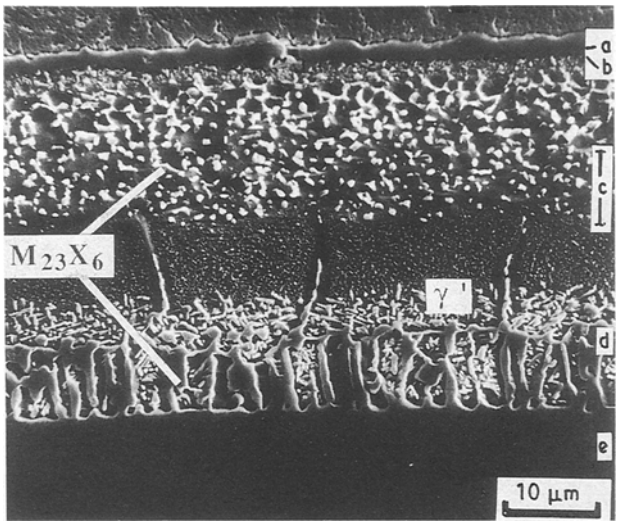

Figure 1 SEM image of general coating microstructure and associated layers (standard-coated sample exposed for 1.5 h at 850 °C in vacuum). (a) oxide, (b) coating surface, (c) main coating, (d) coating transition, and (e) substrate transition and bulk substrate.

With the standard thickness coatings, the coating-transition layer was found to be chromium-rich compared to the substrate-transition layer. In contrast, with thin coatings, the chromium content of these two layers was comparatively even. As a result, very extensive precipitation of $M_{23}X_6$ occurred in the substrate-transition zone of thin coatings, whereas such behaviour was largely confined to the main coating layer of standard coatings. In the case of thin coatings, interlinked networks of $M_{23}X_6$ precipitates (with the same orientations as those in the standard coatings) were produced, either in isolation (at 950 °C) or together with the β-needles (at 850 °C Fig. 2c, d) described in previous work [4].

In summary, $M_{23}X_6$ precipitates form in the transitional and bulk-substrate zones along $\langle 110 \rangle_\gamma$, cube–cube orientation related to the γ.

3.1.2. Precipitation in the coating

Within both standard and thin coatings, extensive precipitation of $M_{23}X_6$ (Fig. 2e) was observed. However, additional features were encountered with the standard coatings which were absent with the thin coatings. Hence the simpler, thin coatings will be discussed first.

3.1.2.1. Thin coatings. $M_{23}X_6$ precipitates were fairly evenly distributed throughout the main layer of the thin coatings. These generally had a more globular morphology than those present in the substrate and no single orientation relationship could be identified

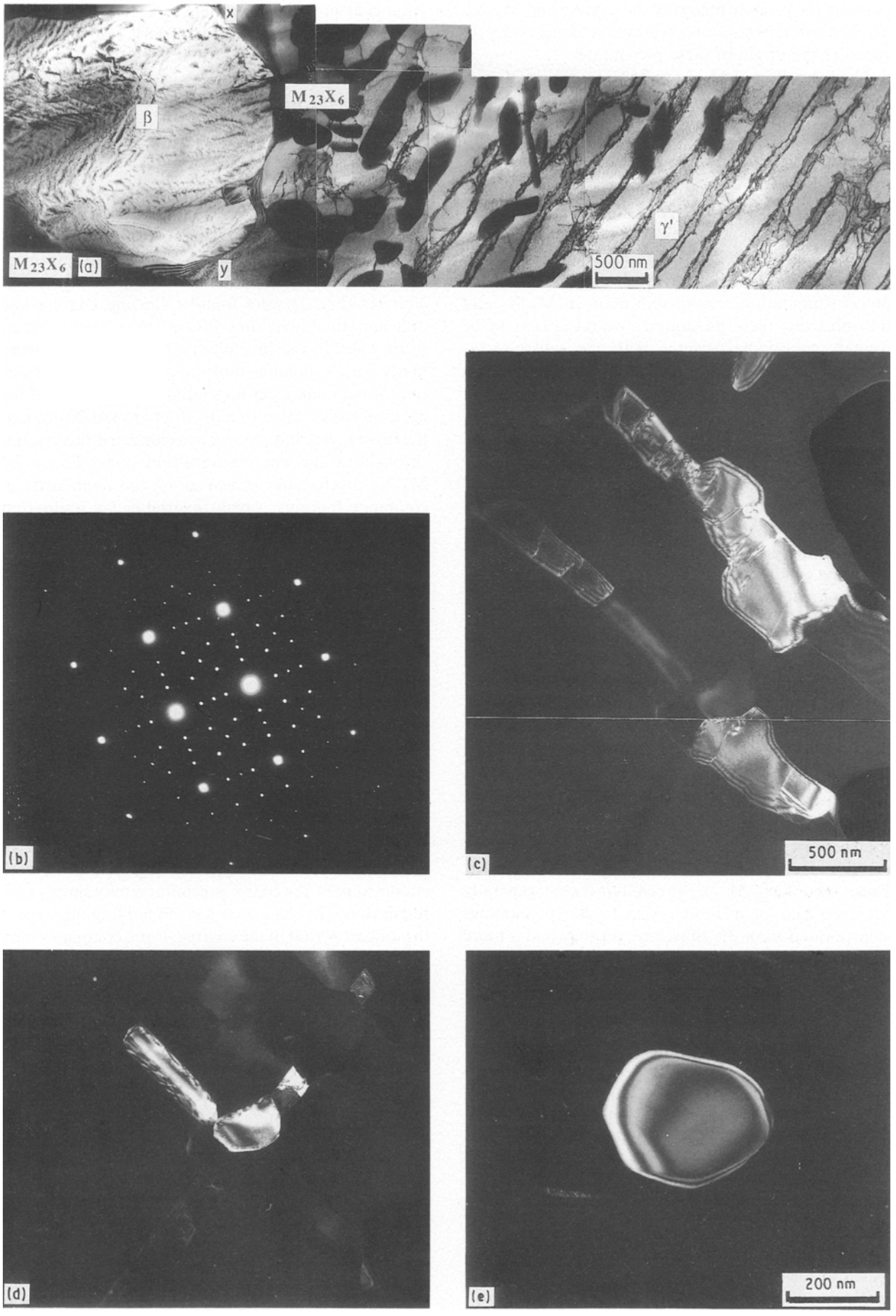

Figure 2 $M_{23}X_6$ precipitation. (a) A bright-field micrograph of $M_{23}X_6$ in the substrate-transition zone of a standard-coated sample in which x–y denotes the coating–substrate interface (sample as-aged). (b) Selected area diffraction pattern (SADP), B = $[1\,0\,0]_\gamma$ showing cube–cube orientation relationship with $M_{23}X_6$ (substrate of thin coated sample, as-aged). (c) and (d) Interlinked network of $M_{23}X_6$ and β in the substrate-transition zone of a thin coated sample, exposed for 1.5 h at 850 °C in air. Dark-field micrographs: (c) g = $(1\,1\,0)_\beta$, and (d) g = $(4\,4\,0)_{M_{23}X_6}$. (e) Dark-field micrograph of $M_{23}X_6$ formed in a thin coating, g = $(4\,0\,0)_{M_{23}X_6}$; sample exposed for 78 h at 850 °C in air.

between the β-phase matrix of the coating and $M_{23}X_6$. To understand these observations it is necessary to consider the origin of these precipitates.

The formation of $M_{23}X_6$ in the coating could arise as a result of either incorporation of substrate precipitates during formation of the coating, or nucleation within the coating following its formation. It was observed that a proportion of the $M_{23}X_6$ precipitates had a constant orientation, which was independent of the orientation of the polycrystalline coating. This is consistent with the incorporation of $M_{23}X_6$ from the substrate into the coating. Although slight curvature of the foils prevented a direct determination of the precise orientation relationship between $M_{23}X_6$ and the substrate, these precipitates would appear to be roughly cube–cube oriented with the substrate (as expected from an incorporated substrate precipitate). A further feature of interest is the difference in morphology between these globular precipitates and the more cuboidal types in the substrate. In general, the coating $M_{23}X_6$ was globular (with a typical diameter of around 200 nm) and rounded in comparison with the cuboidal precipitate in the substrate (although of a generally similar size). In the absence of an orientation relationship between the $M_{23}X_6$ and the β-matrix it would be expected that spheroidal precipitates would be favoured and hence the change to a globular morphology is not surprising.

In addition to any direct influence that these precipitates exert on the properties of the coating, they are also of interest because they act as nucleation sites for primary γ′-precipitates and hence may increase the rate of decomposition of the β-matrix. Subsequent to the formation of primary γ′, further nucleation of $M_{23}X_6$ occurs on the γ′, which then provides sites for further precipitation of $M_{23}X_6$ or γ′ (resulting in the formation of a precipitation cascade, as described elsewhere [4]). The secondary $M_{23}X_6$ formed during the cascades was cube–cube oriented to the γ′-phase. These secondary $M_{23}X_6$ precipitates were generally equiaxed and of a similar size to the precipitates incorporated from the substrate, yet they had a more angular morphology. In addition, a few isolated, intragranular, globular precipitates were observed with a random orientation. Since the substrate $M_{23}X_6$ had a fixed orientation, these precipitates would appear to have been nucleated from the coating matrix (either the β-phase or other Ni–Al phases present during the initial coating stage which are removed during diffusion treatment) rather than incorporated from the substrate. Although substrate grain boundaries were generally dominated by γ′-precipitates any excess grain-boundary area was found to act as a nucleation site for randomly oriented $M_{23}X_6$.

In summary, it can be seen that there are three classes of $M_{23}X_6$ precipitates, which are: (i) incorporated in the coating and with an orientation related to the substrate rather than the coating, (ii) formed on γ′ during the precipitation cascades and cube–cube oriented to the γ′, and (iii) nucleated directly from the coating matrix and randomly oriented. Generally similar behaviour was observed in the coating-transition layer, although in this region the $M_{23}X_6$ was somewhat coarser than in the main layer (typically 500 nm as opposed to 200 nm in diameter). For the surface layer, behaviour similar to that in the main layer was observed, apart from a tendency for nucleation of $M_{23}X_6$ on the β-coating oxide interface (which then acts as a nucleation site for γ′).

3.1.2.2. Standard coatings. In standard coatings the three types of $M_{23}X_6$ precipitation, described above for thin coatings, were also observed in the main coating layer. However, additional coarse $M_{23}X_6$ precipitates (Fig. 1) were found following coating and diffusion treatment and further post-coating treatment. These coarse precipitates occurred in two forms, firstly with a globular morphology in the upper portion of the main layer (extending from the end of the coating-surface layer to a depth of around 20 μm into the main layer) and secondly as elongated precipitates throughout the coating-transition zone. Elongated $M_{23}X_6$ precipitates formed along the boundaries of columnar β-grains, which invariably lay approximately perpendicular to the substrate surface (regardless of the orientation of the substrate) with apparently random crystallographic orientations.

In the coating-transition zone, marked chromium enrichment (compared to the rest of the coating) was produced, presumably due to chromium rejection by the growing coating during coating formation. Hence, preferential formation of chromium-rich phases might be expected. However, for the precipitates in the main layer, no such chromium enrichment was observed and a different explanation may be formulated. As these precipitates generally had a fixed orientation, it would appear that most of these coarse phases were produced by incorporation of substrate $M_{23}X_6$, which had subsequently undergone growth (as a result of chromium rejection from the coating matrix). In these circumstances, the coarse precipitates may simply represent those that had, after a given holding time, spent the longest period in the coating. For a coating formed predominantly by inward diffusion (as in the present case [5, 6]), such precipitates would lie towards the outside of the coating, since this region is formed first. This correlates with the observed behaviour of the coarse $M_{23}X_6$ phases.

In the standard coatings, unlike the thin coatings, the formation of $M_{23}X_6$ was superceded by other precipitation (although the existing $M_{23}X_6$ precipitates remained stable) following moderate exposure. The precipitation of $M_{23}X_6$ alone was observed after coating and diffusion treatment; however, the formation of other phases had commenced after the completion of the 16 h at 870 °C ageing stage. This was rapidly followed by the termination of $M_{23}X_6$ precipitation which occurred after a further treatment of 1.5 h exposure at 850 °C. In coatings on single-crystal superalloys (which have low carbon contents), the formation of a phase such as $M_{23}X_6$ which contains significant quantities of carbon is unlikely to be sustainable for long periods and hence the formation of other carbon-free or leaner carbon phases is to be

expected, at least in standard coatings where substantial $M_{23}X_6$ precipitation was observed after the diffusion-treatment stage. In subsequent sections, the changes in the precipitation behaviour in standard coatings with post-coating treatment will be examined.

3.2. α-Cr precipitation

Following the 16 h ageing treatment, at 870 °C, a distribution of fine, coherent precipitates, consisting essentially of chromium, was observed in the β-phase. Precipitate-free zones were produced in the chromium-depleted regions surrounding intragranular $M_{23}X_6$ precipitates and around β–β-boundaries on which $M_{23}X_6$ had precipitated (Fig. 3). The chromium-rich precipitates were spheroidal, usually with diameters of around 100 nm or less. Occasional coarser precipitates (typically of around 300–400 nm in diameter), with lower coherency with the β compared to the fine precipitates, were observed both intragranularly and on β-grain boundaries (and low-angle β-boundary triple points). These relatively coarse precipitates became more common with further exposure (especially after 78 h at 850 °C).

The precipitating phase was found to contribute strongly to the body-centred-cubic (b.c.c.) basis reflections, but only weakly to the CsCl-type superlattice of the B2 β-phase. The b.c.c. basis of NiAl (a_0 = 287–289 pm in binary NiAl) is very closely matched to the lattice of α-Cr (a_0 = 288 pm) and essentially the precipitating phase can be regarded as α-Cr cube–cube orientation related to the β-matrix. Phenomenologically, this region consists of a mirror image of the substrate, since the superlattice constitutes the matrix phase and the basis a coherent second phase.

The formation of occasional isolated "chromium grains" has been described by Shen *et al.* [1] in their study of aluminized superalloys. However, the only example found in the literature for the generalized precipitation of α-Cr within the β-phase is in binary NiAl doped with chromium, as described by Miracle *et al.* [7]. Extensive precipitation of α-Cr would not be surprising in a system in which other elements which readily form intermetallics with chromium (such as molybdenum) are absent; however, intermetallic formation might be expected in a complex coating. Nonetheless, an analogous process is observed in ferritic stainless steels, including those containing molybdenum and titanium [8, 9], in which the formation of chromium-rich clusters (denoted as α′) takes place. In those materials, nucleation occurs within a miscibility gap, outside a region of spinodal decomposition [10]. In the present investigation, it was noted that the "tweed" microstructure and associated diffraction anomalies (which are common features of nickel-rich β in the Ni–Al binary system [11, 12]) were considerably more prominent in thin coatings, which did not undergo spheriodal α-Cr precipitation, than in standard coatings for which spheriodal α-Cr precipitates were produced. Indeed, in addition to the orthogonal tweed microstructure, further spinodal-like unidirectional

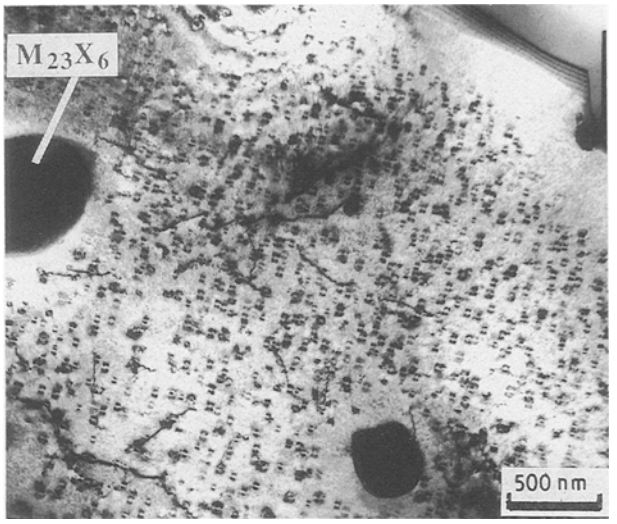

Figure 3 Bright-field micrograph of α-Cr precipitation in a standard coating (sample, as-aged).

stripes were observed from thin coating β (although no further diffraction anomalies were noted); these stripes were absent in the thicker coatings. Thus, although further investigation is required, there may exist a parallel between the α′ and α-Cr precipitation processes.

In terms of the implications for coating properties, the addition of chromium is predicted to result in a reduction in the anti-phase boundary (APB) energy of the β-phase [13]. Any tendency toward reduced order would be beneficial from the stand-point of promoting coating ductility at low temperatures. In the highly ordered binary NiAl phase, superlattice dislocations are not formed and only perfect dislocations with $a_0 < 0\,0\,1 >$ Burgers vectors usually occur [14], with the result that an insufficient number of slip systems exists to allow ductility in a polycrystalline coating. Miracle *et al.* [7] have observed that chromium additions to binary NiAl promote the formation of $< 1\,1\,1 >$ Burgers vectors (presumably by allowing the formation of APBs). Nonetheless, this is not accompanied by a significant improvement in ductility. The workers were unclear, however, as to the extent to which the presence of the α-Cr precipitate influenced this situation. Although detailed characterization was not performed, it was observed in the present investigation that the α-Cr precipitates were sites of preferential dislocation activity, and hence it seems likely that a positive, rather than negative, effect on ductility would result from the presence of these phases.

3.3. Precipitation of σ and other molybdenum rich phases

3.3.1. Precipitation in standard coatings

In addition to any direct effect of the α-Cr reaction on the microstructure of standard thickness coatings, the formation of this phase has the indirect effect of decreasing the ratio of chromium to molybdenum in the coating matrix. This chemical change promotes the formation of phases containing significant quantities of molybdenum in the standard thickness coatings.

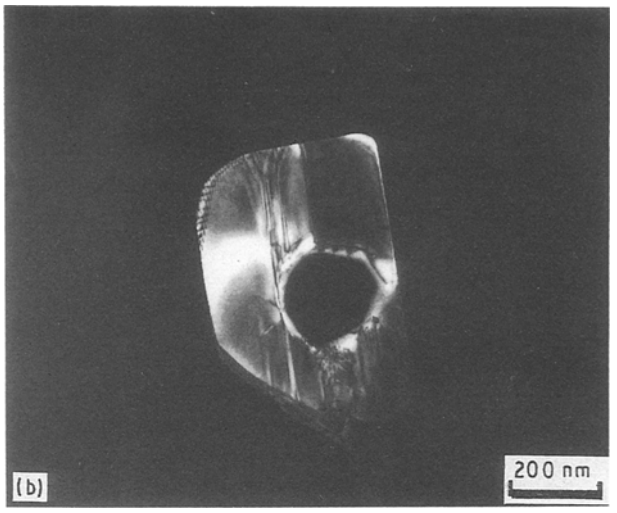

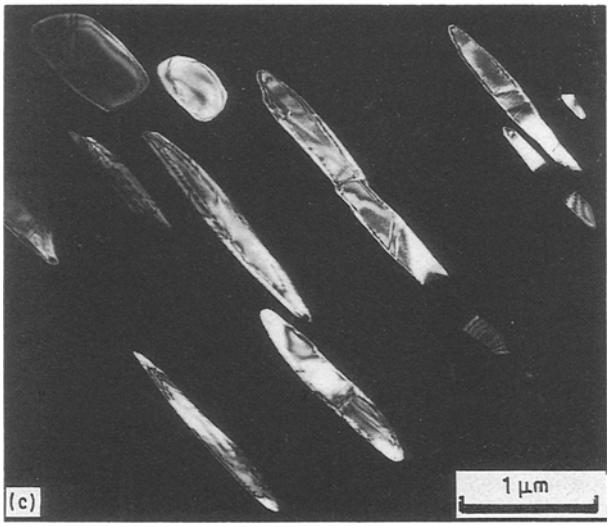

Figure 4 σ-phase precipitation in standard thickness coatings (dark-field micrographs). (a) SADP showing σ-phase precipitation in the β-matrix ($B \approx [1\,1\,1]_\beta$; sample exposed for 1.5 h at 850 °C in air). (b) In the coating on an MX precipitate (dark field, $g = (0\,0\,\bar{2})_\sigma$ sample exposed for 1.5 h at 850 °C in air). (c) In the substrate (dark field, $g = (0\,\bar{2}\,\bar{2})_\sigma$; sample exposed for 138 h at 850 °C in air).

The most prominent of these phases was found to be σ (rich in chromium and molybdenum) which was first produced after 1.5 h post-ageing exposure at 850 °C and continued throughout the timescale examined (up to 138 h exposure at 850 °C). The formation of σ, as angular precipitates often with extensive stacking faults, was observed throughout the coating. A marked orientation relationship (Fig. 4a) was observed between the σ- and β-phases, such that: $[1\,1\,1]_\beta$ was parallel to $[1\,1\,0]_\sigma$, and $(\bar{1}\,1\,0)_\beta$ was parallel to $(1\,\bar{1}\,0)_\sigma$.

The σ-phase was found to nucleate either directly from the β or on globular MX-type precipitates (in which M was almost entirely titanium with traces of vanadium, and X is presumed to be carbon), as shown in Fig. 4b. The MX phases were apparently of a random orientation. Although no direct evidence was obtained for the origin of the MX phases, similar phases were observed in the substrate. Thus, it seems likely that the MX was incorporated in the coating during its formation. σ-phase formation also occurred on coarsened α-Cr precipitates, especially on β-grain boundaries, but not on the fine, coherent α-Cr.

Simultaneously with the formation of σ-phase intermetallics, some precipitation of M_6X (with M being chromium and molybdenum and X, presumably, carbon) was observed. Generally, this occurred directly from the β-matrix (Fig. 5), although precipitation on MX phases was also observed. M_6X formation took place at the completion of $M_{23}X_6$ precipitation and onwards (i.e. after 1.5 h exposure at 850 °C) and the change from carbon and chromium rich $M_{23}X_6$ to M_6X with lower levels of carbon and a decreased ratio of chromium to molybdenum (and a reduced amount of precipitation) would appear to reflect depletion of both the limited carbon supply and loss of chromium to the α-Cr precipitates.

Unlike $M_{23}X_6$, it was found that M_6X maintained a cube–cube orientation relationship with the β (Fig. 5c). This difference, presumably, reflects the different origins of the M_6X and $M_{23}X_6$. Whereas M_6X is formed directly from β, it was noted earlier that $M_{23}X_6$ arises from the following: incorporation in the coating, precipitation on γ′ and possibly formation from matrix phases other than β (in the high-activity aluminization process, phases richer in aluminium are initially formed [15]). In contrast, the difference in lattice parameter between M_6X and $M_{23}X_6$ is unlikely to account for the failure to establish an orientation relationship between the $M_{23}X_6$ and β-phases. The lattice parameter for M_6X (115 pm in the present work) is approximately four times that of β and, compared to that of $M_{23}X_6$ (105 pm), produces a better fit with the β-matrix. However, the mismatch between the β- and $M_{23}X_6$-phase lattice parameters is only some 10% and this should not preclude the establishment of an orientation relationship between β and $M_{23}X_6$.

Simultaneously with M_6X, precipitation of the chromium- and molybdenum-containing χ-phase was observed (following 1.5 h exposure at 850 °C). This phase formed directly from β and was oriented to β as follows: $[1\,1\,0]_\beta$ parallel to $[1\,1\,0]_\chi$, and $(0\,0\,\bar{1})_\beta$ parallel to $(\bar{1}\,1\,3)_\chi$. Although precipitation in association with M_6X was also observed. In austenitic stainless steels

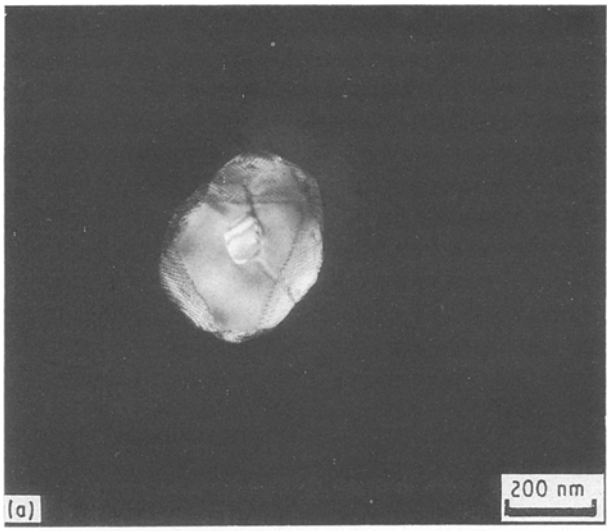

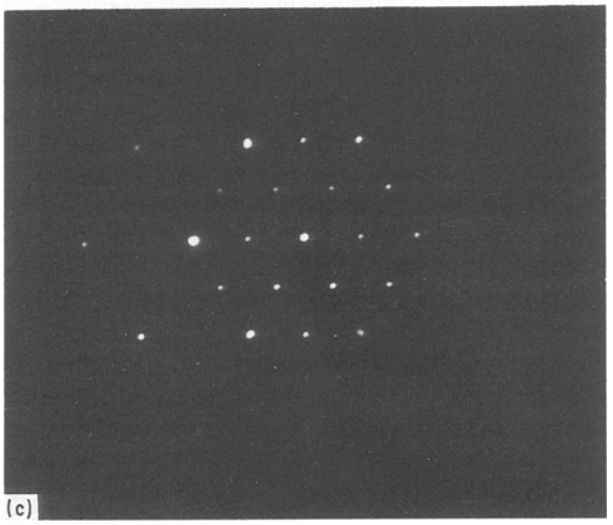

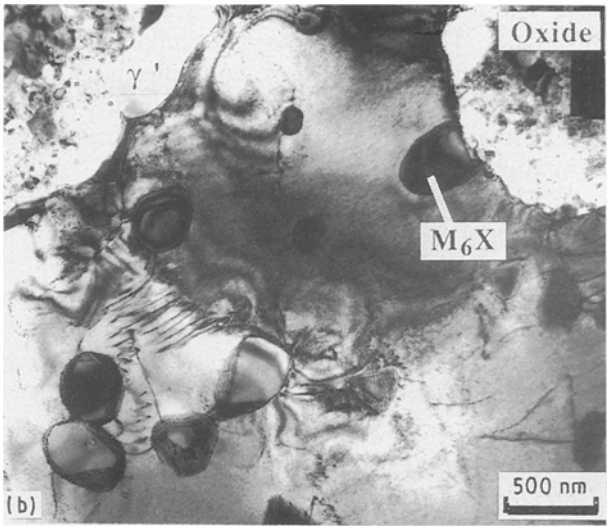

Figure 5 M_6X precipitation in a standard coating exposed for 138 h at 850 °C in air. (a) Dark-field micrograph ($g = (\bar{2}\,2\,0)_{M_6X}$), (b) bright-field micrograph, (c) SADP ($B = [1\,1\,1]_\beta$) showing cube–cube orientation of M_6X and β.

the χ-phase is either a chromium/molybdenum bearing intermetallic or $M_{18}C$, which fits in with the general trend of precipitation described above. Although the phases discussed so far contain significant molybdenum, a further type of precipitate was simultaneously observed on β-grain boundaries (and low-angle-boundary triple points). This precipitate was found to consist of chromium and titanium and to be of the Laves type and thus is presumed to be the Cr_2Ti-phase. In the later stages of precipitation (i.e. after 16 h exposure at 850 °C), intragranular needles of this phase were produced. The occurrence of this titanium-rich phase might be linked to chromium depletion from the β-phase in a manner similar to that suggested for the molybdenum-bearing phases.

3.3.2. Precipitation in the substrate below standard coatings

There was a general tendency for a change from the precipitation of $M_{23}X_6$ to that of σ in the substrate below the standard coatings during post-coating treatment (as was the case within the coating). Morphologically, the σ-phase (Fig. 4c) was similar to $M_{23}X_6$ (although slightly more rounded) and also formed along the $< 1\,1\,0 >_\gamma$ directions. The following orientation relationship was observed between the σ- and γ-phases: $[1\,1\,0]_\gamma$ was parallel to $[1\,1\,0]_\sigma$, and $(1\,\bar{1}\,1)_\gamma$ was parallel to $(0\,0\,\bar{1})_\sigma$. This is commonly observed in superalloys. This type of transformation has been well documented in some early superalloys, although the extent and rate of σ precipitation was greatly enhanced over that usually encountered, due to disturbance of the chemistry of the substrate as a result of coating. In the substrate, the σ-precipitates were found, in the later stages of exposure (after 78 h at 850 °C), to begin to replace $M_{23}X_6$, rather than augmenting $M_{23}X_6$ precipitation as in the coating.

Conclusions

An examination has been made of the precipitation of chromium-containing phases in high-activity pack-aluminized single crystals of a nickel-base superalloy.

1. In the case of precipitation in the substrate, $M_{23}X_6$ and σ are observed. Whilst these phases are familiar in superalloys the compositional disturbance produced by coating enhances the rate of $M_{23}X_6$ precipitation and (in standard thickness coatings) results in the formation of σ-phase.

In the coating, a more complex series of developments was observed (with standard coatings) and these will now be summarized.

2. The first chromium-containing phase to form in the coating was found to be $M_{23}X_6$. The morphology and orientation relationships of this phase varied as a function of the origin of an individual precipitate (from incorporation from the substrate, nucleation from the coating matrix or nucleation on γ′ precipitates in the coating).

3. In this low carbon, single-crystal system, the formation of the comparatively carbon-rich $M_{23}X_6$ phase is gradually superceded by other phases of a lower carbon content.

4. The first phase to form after $M_{23}X_6$ is an α-Cr precipitate. The α-Cr phase is very similar to the b.c.c. basis of the β-phase and this reaction effectively results in localized removal of the superlattice of the β-matrix. The formation of α-Cr bears some similarity to the formation of α′ in ferritic stainless steels.

5. The formation of the α-Cr precipitates reduces the ratio of available-chromium-to-molybdenum in the β-phase and encourages the precipitation of phases which are comparatively rich in molybdenum. This resulted in the formation of σ, χ and M_6X.

6. The occurrence of a chromium–titanium Laves phase (presumably Cr_2Ti) has been observed.

Acknowledgements

The authors wish to acknowledge and record the co-operation of the late Dr T. N. Rhys-Jones of Rolls–Royce Plc. Grateful thanks are due to Mr T. J. Marrow, formerly of the University of Cambridge now at the University of Oxford, for drawing the authors' attention to various pieces of literature on the precipitation of α′ in iron-based systems. Financing of the research project and of W. F. G. by Rolls–Royce Plc. and the Science and Engineering Research Council is acknowledged with thanks. J. E. K. is grateful to British Gas Plc. and the Fellowship of Engineering for financial support.

References

1. P. SHEN, D. GAN and C. C. LIN, *Mater. Sci. Engng.* **78** (1986) 171.
2. P. SHEN, D. GAN and C. C. LIN, *Mater. Sci. Engng.* **78** (1986) 163.
3. "Ternary alloys, a comprehensive compendium of evaluated constitutional data and phase diagrams", Vol. 4, Edited by G. Petzow and G. Effenberg, (VCH Publishers, New York, 1991) p. 409.
4. W. F. GALE and J. E. KING, *Metall. Trans.* A **23** (1991) 2657.
5. S. R. LEVINE and R. M. CAVES, *J. Electrochem. Soc.* **121** (1974) 1051.
6. A. J. HICKL and R. W. HECKEL, *Metall. Trans. A* **6** (1975) 431.
7. D. B. MIRACLE, S. RUSSELL and C. C. LAW, *Mater. Res. Soc. Symp. Proc.* **133** (1989) 225.
8. P. J. GROBNER, *Metall. Trans.* **4** (1973) 251.
9. P. JACOBSSON, Y. BERGSTRÖM and B. ARONSSON, *Metall. Trans. A* **6** (1975) 1577.
10. T. DE NYS and P. M. GIELEN, *Metall. Trans.* **2** (1971) 1423.
11. I. M. ROBERTSON and C. M. WAYMAN, *Metall. Trans. A* **15** (1984) 1353.
12. H. C. LIU, E. CHANG and T. E. MITCHELL, in Proceedings of the 39th. Annual Meeting of the Electron Microscopy Society of America, Atlanta 1981, (Claitors Publishing Division, Baton Rouge, 1981) pp. 58–59.
13. T. HONG and A. J. FREEMAN, *Mater. Res. Soc. Symp. Proc.* **133** (1989) 75.
14. R. J. WASILEWSKI, S. R. BUTLER and J. E. HANLON, *Trans. Metall. Soc. AIME* **239** (1967) 1357.
15. J. T. BOWKER, Aluminide Coatings on Nickel-Base Superalloys, PhD thesis University of Sheffield (1978).

Received 7 January
and accepted 2 October 1992